Revision 1

The S content of silicate melts at sulfide saturation: new experiments and a model incorporating the effects of sulfide composition

Duane J. Smythe*, Bernard J. Wood and Ekaterina S. Kiseeva

Department of Earth Sciences, University of Oxford, South Parks Road, Oxford, OX1 3AN, UK.

* E-mail: duane.smythe@earth.ox.as.uk

Abstract

The extent to which sulfur dissolves in silicate melts saturated in an immiscible sulfide phase is a fundamental question in igneous petrology and plays a primary role in the generation of magmatic ore deposits, volcanic degassing and planetary differentiation. In igneous systems sulfide melts can be described as FeS-NiS-$CuS_{0.5}$ solutions with Fe/(Fe+Ni+Cu) significantly less than 1. Despite the presence of Ni and Cu in the sulfide, however most experimental studies to date have concentrated on the effects of silicate melt composition on sulfur solubility and have used essentially pure FeS as the sulfide liquid.

We have carried out 49 new experiments at pressures of 1.5-24 GPa and temperatures of 1400 to 2160°C in order to investigate the effects of sulfide composition on sulfur solubility as well as extending the pressure and temperature ranges of the available

data on sulfide saturation. We find that, in the compositional range of most igneous sulfide melts (Fe/(Fe+Ni+Cu) >0.6) sulfur solubility decreases linearly with Fe content such that at Fe/(Fe+Ni+Cu) of 0.6, the sulfur content at saturation is 0.6 times the value at pure FeS saturation. At lower values of Fe/(Fe+Ni+Cu) deviations from this ideal solution relationship need to be taken into consideration, however. We have treated these nonidealities by assuming that FeS-NiS-$CuS_{0.5}$ liquids approximate ternary regular solutions.

We have fitted our data, together with data from the literature (392 in total) to equations incorporating the effects of silicate melt composition, sulfide liquid composition and pressure on the solubility of sulfur at sulfide saturation $[S]_{SCSS}$. The temperature dependence of $[S]_{SCSS}$ was assumed either to be an unknown or was taken from 1 bar thermodynamic data. The most important best-fit silicate melt compositional term reflects the strongly positive dependence of $[S]_{SCSS}$ on the FeO content of the silicate melt. The best-fit value of this parameter is essentially independent of our assumptions about temperature dependence of $[S]_{SCSS}$ or the solution properties of the sulfide.

All natural compositions considered here exhibit positive dependences of $[S]_{SCSS}$ on temperature and negative dependences on pressure, in accord with previous studies using smaller datasets.

Keywords: sulfur solubility, silicate melt, sulfide, MORB

Introduction

The solubility of sulfur in silicate melts is a subject which attracts the attention of metallurgists interested in the conditions under which immiscible sulfide mattes segregate from silicate slags (e.g. Fincham and Richardson 1954) and of geologists concerned with the behaviour of sulfur and chalcophile elements during igneous processes. In the former case, the work of Fincham and Richardson led to a quantitative model for the solubility of S (as S^{2-}) and its dependence on oxygen and sulfur fugacities. In the latter the dependence of sulfur solubility on silicate melt composition and temperature control volcanic degassing (Fischer et al., 1998; Wallace, 2005) and the formation of magmatic sulfide ore deposits (Li and Ripley, 2005; Mungall, 2007). Sulfide liquid precipitates during the differentiation of MORB (Peach et al., 1990) thereby controlling the concentrations of chalcophile elements such as Cu, Ag, Tl and the PGE's in the crystallising silicate melts. Precipitation of immiscible sulfide and sulfur solubility may also be important during planetary accretion and differentiation (Holzheid and Grove, 2002; Wood et al., 2014). For these reasons there have been numerous experimental investigations of the processes that control the incorporation of sulfur in naturally-occurring silicate melts (e.g.Shima and Naldrett, 1975; Mavrogenes and O'Neill, 1999; O'Neill and Mavrogenes, 2002; Li and Ripley, 2005; Liu et al., 2007).

At relatively low oxygen fugacities (i.e. below that of the fayalite-magnetite- quartz (FMQ) buffer) Fincham and Richardson (1954) proposed that sulfur dissolves in silicate melts as S^{2-} and that it substitutes for oxygen on the anion sublattice via the reaction

$$O^{2-} + \frac{1}{2}S_2 = S^{2-} + \frac{1}{2}O_2 \qquad (1)$$

In silicate melts the concentrations of O^{2-} are generally two or more orders of magnitude greater than those of S^{2-}, even at sulfide saturation. Given this constraint we can take the O^{2-} concentration on the anion sublattice to be constant and rearrange the equilibrium constant for reaction (1) to yield the Fincham - Richardson relationship (Fincham and Richardson, 1954):

$$\ln C_S = \ln [S] + \frac{1}{2}\ln(fO_2/fS_2) \qquad (2)$$

In Equation (2) C_S is the sulfide capacity of the melt (analogous to the equilibrium constant), and [S] is the concentration of sulfur, usually in ppm. Fincham and Richardson (1954) experimentally verified the relationship of Equation (2) by measuring sulfur contents of silicate melts in the system CaO-Al_2O_3-SiO_2 at fixed values of fS_2 and fO_2. In the geologic literature, most interest has been on the conditions of sulfide saturation and precipitation of sulfides from basaltic and related liquids (e.g. Haughton et al. 1974, Katsura and Nagashima, 1974, Wallace and Carmichael, 1992). Nevertheless, O'Neill and Mavrogenes (2002) broadened the scope of study by measuring the concentrations of S in 19 melts in the geologically relevant system CaO-MgO-Al_2O_3-$SiO_2 \pm TiO_2 \pm FeO$. They showed that, at 1400ºC and known fS_2 and fO_2 between -3.36 and 1.59, and -10.92 and -6.78, respectively, all 19 melts obey the Fincham - Richardson relationship.

Because of its geologic importance and the large number of data currently available, our study has been primarily concerned with the conditions of sulfide saturation in silicate melts of different composition over wide ranges of pressure and temperature.

In this context we begin by assuming that the Fincham - Richardson relationship applies to all melts of geologic interest. Equilibrium between sulfide and silicate melt may then be described in terms of the reaction:

$$\mathrm{FeO}^{silicate} + \frac{1}{2}\mathrm{S}_2 = \mathrm{FeS}^{sulfide} + \frac{1}{2}\mathrm{O}_2 \qquad (3)$$

for which, at equilibrium we have:

$$\Delta G^\circ = -RT \ln \frac{a_{\mathrm{FeS}}^{sulfide} \cdot f\mathrm{O}_2{}^{1/2}}{a_{\mathrm{FeO}}^{silicate} \cdot f\mathrm{S}_2{}^{1/2}} \qquad (4)$$

where ΔG° is the standard state free energy change of reaction (3) and activities and fugacities of the 4 components have their usual symbols. Rearranging Equation (4) we obtain:

$$\frac{\Delta G^\circ}{RT} = \ln a_{\mathrm{FeO}}^{silicate} - \ln a_{\mathrm{FeS}}^{sulfide} - \ln \frac{f\mathrm{O}_2{}^{1/2}}{f\mathrm{S}_2{}^{1/2}} \qquad (5)$$

We may now substitute from Equation (2) for the ratio of oxygen to sulfur fugacity as follows:

$$\ln[\mathrm{S}]_{\mathrm{SCSS}} = \frac{\Delta G^\circ}{RT} + \ln C_{\mathrm{S}} + \ln a_{\mathrm{FeS}}^{sulfide} - \ln a_{\mathrm{FeO}}^{silicate} \qquad (6)$$

In Equation (6), $[S]_{SCSS}$ refers to the sulfur content of the silicate melt at sulfide saturation and $a_{FeS}^{sulfide}$ and $a_{FeO}^{silicate}$to the activities of FeS and FeO components in sulfide and silicate melts respectively.

Inspection of Equation (6) enables us to consider, qualitatively, the important influences on the sulfur content of any particular melt at sulfide saturation. The standard state free energy change of the reaction $\Delta G°$ depends on pressure and temperature which requires that $[S]_{SCSS}$ is also *P-T* dependent. Measurements of C_S, and of sulfur concentrations at sulfide saturation have demonstrated that C_S is composition-dependent, most notably varying strongly and positively with the FeO content of the silicate melt. In contrast, the term in $a_{FeO}^{silicate}$ requires an increase in S content with *decreasing* FeO content of the silicate melt. There is thus a trade-off between the positive contribution of FeO to $[S]_{SCSS}$ and the negative effect of $a_{FeO}^{silicate}$ on sulfur solubility which leads to a theoretical U-shape of a plot of $[S]_{SCSS}$ versus FeO content (O'Neill and Mavrogenes, 2002 fig 21). Thus, most attempts to model $[S]_{SCSS}$ have emphasized the major compositional terms for the silicate melt. Pressure effects have also been shown to be very important (e.g Holzheid and Grove, 2002, Mavrogenes and O'Neill, 1999). Much less attention has been paid to the composition of the sulfide melt, however, as represented by $a_{FeS}^{sulfide}$ in Equation (6) (Ariskin, et al. 2013). Instead, almost all experimental measurements to date have used pure FeS as the sulfide phase, with the implicit assumption that lowering $a_{FeS}^{sulfide}$ by diluting Fe with other cations has no effect on sulfur solubility. Equation (6) indicates, however, that S solubility must decrease as FeS activity decreases, meaning that, in general it must be lower than is implied by pure FeS saturation. Immiscible droplets of sulfide in basalt contain up to 18 and 20 wt% Ni and Cu respectively (Francis, 1990; Patten et

al 2013), which means that the sulfide is only about 60% FeS by mole. Despite these observations, and the appreciable effort made, to date, to determine S solubility in silicate melts, there are few data enabling the effects of dilution of Fe by other cations to be evaluated. One major goal of the present experimental study is to address this fundamental question and to quantify the effects of Ni and Cu substitutions on FeS activity and hence on $[S]_{SCSS}$ in relevant natural compositions. To this end we have performed 49 new experiments at 1.5 to 24 GPa and 1400 to 2160ºC with immiscible sulfide melt compositions ranging from pure FeS to nearly pure NiS and $CuS_{0.5}$. The new data enable us to quantify the effects of Ni and Cu substitution for Fe as well as providing the basis, together with literature data, for determining the effects of pressure and temperature and silicate melt composition on $[S]_{SCSS}$.

Experimental and Analytical Procedures

Experimental methods

Starting materials consisted of mixtures of ~50% $(Fe,Ni,Cu_2)S$ and ~50% synthetic silicate, by weight. The sulfide component consisted of mixtures of analytical grade FeS, NiS and $CuS_{0.5}$. The silicate constituent was in many cases a composition close to the 1.5 GPa eutectic composition in the system anorthite–diopside–forsterite ($An_{50}Di_{28}Fo_{22}$) (Presnall et al., 1978) with variable $Fe_{0.95}O$ added , but a range of basaltic, andesitic and komatiitic compositions was also employed. All components were added to these mixtures either as analytical grade oxides (SiO_2, TiO_2, Al_2O_3, MgO, Fe_2O_3, MnO_2, P_2O_5) or as carbonates (Na_2CO_3, K_2CO_3, $CaCO_3$). The silicate mixtures were pelletized and decarbonated at 950°C for 2 hours. After that the Fe_2O_3

was added, mixtures were reground, pelletized and reduced in a CO-CO_2 atmosphere for 2 hours at 1000°C and an oxygen fugacity approximately 2 log units above the IW buffer. Silicate and sulfide constituents were intimately mixed in approximately 50:50 proportions prior to each experiment. Additional Fe (as $Fe_{0.95}O$) was added to some experiments in order to increase FeO activity. The starting mixtures were dried at 110°C immediately before the experiment.

Most experiments were performed at 1.5 and 2.5 GPa using a 12.7 mm diameter Boyd-England-type piston-cylinder apparatus at the University of Oxford. The sample cell employed an outer sleeve of pressed CaF_2, a graphite heater of 8 mm outside and 6 mm inside diameter and internal parts of machineable MgO. Most experiments were performed in 3.0 mm O.D., 1 mm I.D. graphite capsules, a subset of which were sealed in Pt outer capsules. A few experiments were performed in SiO_2 glass capsules. Experiment durations were fixed at times substantially longer than those required to reach sulfide-silicate and metal-silicate partitioning equilibrium in capsules of 1 mm inner diameter {Tuff, et al. 2011;Kiseeva and Wood 2013) For piston-cylinder experiments at 1500°C and higher temperatures the outer calcium fluoride sleeve was replaced by an outer thin-walled $BaCO_3$ cylinder with an inner sleeve of SiO_2 glass. All temperatures were monitored and controlled using $W_{95}Re_5$-$W_{74}Re_{26}$ thermocouples housed in alumina sheaths and separated from the capsule by a 0.6 mm thick alumina disk. Experiments at 5.5 and 7 GPa employed a Walker-type multianvil apparatus and cast MgO-based octahedra. The furnace assemblies consisted of straight graphite heaters inside ZrO_2 sleeves and the capsules were, as before fabricated from graphite. One experiment was performed at 24 GPa/ 2160°C at the Bayerisches Geoinstitut, Universität Bayreuth. In this case the capsule was made of

single-crystal MgO. As for the piston-cylinder experiments, all multianvil experiments employed W-Re thermocouples, in these cases in direct contact with the capsule. Experimental run conditions and starting compositions are given in Table 1.

Analytical techniques

Experimental products were analysed using a JEOL JXA8600 electron microprobe housed in the Department of Archaeology at the University of Oxford. Silicate glasses were analyzed by wavelength dispersive spectroscopy (WDS) employing a 15 kV accelerating voltage and a 35-40 nA beam current. The spot was typically defocused to10 μm diameter. Standards used for silicate glass analysis include natural wollastonite (Si, Ca), natural jadeite (Na, Al) synthetic periclase (Mg), rutile (Ti), hematite (Fe), $NdPO_4$ (P), orthoclase (K) and galena (S). Natural almandine and natural S-bearing glasses VG-1 and L17 were used as secondary standards for S. Counting times were as follows: 30 s peak and 15 s background for major elements (Si, Al, Ca, Mg, Fe); 60 s peak and 30 background for minor elements (Na, K, Ti, P); 180 s peak and 90 s background for S. Analysis of sulfides by WDS used a 15 kV accelerating voltage, a 20 nA beam current and a defocused beam, generally of 10 μm, but occasionally of 15μm diameter for the most heterogeneous quenched liquids. Standards for sulfide analysis consisted of Hematite (Fe, O), galena (S), Ni metal (Ni) and Cu metal (Cu). Count times were 30 s peak and 15 s background for Fe and S, and 60 s peak and 30 s background for Ni and Cu. Oxygen in the sulfide was measured using the K_α peak and a LDE pseudocrystal (Kiseeva and Wood, 2013) with count times of 100 s peak and 50 s background. There was no evidence of strong heterogeneity in oxygen contents, as might have been expected if there were large

grains of quenched oxide within the sulfide blobs. Electron microprobe analyses of silicate and sulfide run products are provided in Table 2.

Results

O'Neill and Mavrogenes (2002) followed Haughton et al. (1974) in treating the measured sulfide capacity as a parameter with simple dependence on the mole fractions X_M of the single metal oxide components (SiO_2, $AlO_{1.5}$, MgO etc)

$$\ln C_S = A_0 + \sum_M X_M A_M / T \qquad (7)$$

The rationale for this approach is that the A_M are related to the differences between the standard state free energies μ° of oxide and sulfide components of the cations of interest (ie MgO, MgS, $Si_{0.5}O$, $Si_{0.5}S$ etc). This gives the following theoretical form for C_S:

$$\ln C_S = -\ln \gamma_S + \sum_M X_M (\mu^o_{M_zO} - \mu^o_{M_zS})/RT \qquad (8)$$

In Equation (8), $(\mu^o_{M_zO} - \mu^o_{M_zS})$ is the standard state free energy difference between oxide and sulfide components of M and γ_S is the activity coefficient of S in the silicate melt. Replacing C_S in Equation (6) with the form of Equation (7) leads to:

$$\ln[S]_{SCSS} = \frac{\Delta G^\circ}{RT} + A_0 + \sum_M X_M A_M / T + \ln a_{FeS}^{sulfide} - \ln a_{FeO}^{silicate} \qquad (9)$$

O'Neill and Mavrogenes (2002) used tabulated thermodynamic data to obtain ΔG° at 1 bar then regressed their C_S data at 1400°C and 1 bar to an equation of similar form to (8) except, since their experiments were isothermal, the dependence of the compositional $X_M A_M$ terms on temperature ($X_M A_M/T$) was ignored. If we use their results at face value, all of the regressed A_M terms are positive and ΔG° has a negative temperature dependence. This means that $[S]_{SCSS}$ should *decrease* with increasing temperature irrespective of whether or not we treat the $X_M A_M$ terms as having dependences on reciprocal temperature. All observations to date, however, including our own, demonstrate that $[S]_{SCSS}$ *increases* with increasing temperature. This means either that the temperature dependence of ΔG° derived from tabulated thermodynamic data is profoundly in error or that the $X_M A_M$ terms of Equation (9) are predominantly negative. Although we consider that the former is unlikely, we have treated the data in two fundamentally different ways in order to resolve this issue. Firstly, we treated ΔG° and its temperature and pressure dependences as unknowns. In this case we divide $\Delta G^\circ/RT$ into enthalpy (ΔH°), entropy (ΔS°) and molar volume terms (ΔV°) as follows:

$$\frac{\Delta G^\circ}{RT} = \frac{\Delta H^\circ}{RT} - \frac{\Delta S^\circ}{R} + \frac{P\Delta V^\circ}{RT} = \frac{A}{T} + B + \frac{CP}{T} \qquad (10)$$

Combining Equations (9) and (10) yields,

$$\ln[S]_{SCSS} = \frac{A}{T} + B' + \frac{CP}{T} + \sum_M X_M A_M /T \; + \ln a_{FeS}^{sulfide} - \ln a_{FeO}^{silicate} \qquad (11)$$

where B' is the sum of the entropy term in Equation (10) and A_0 from Equation (7). We now use Equation (11) as one of the bases for our regression of $\ln[S]_{SCSS}$ as a function of compositional terms A_M, pressure and temperature.

Our second approach was to assume that the tabulated thermodynamic data are correct and to adopt the 1 bar values of $\Delta G°$ given by O'Neill and Mavrogenes (2002). This gives the following equation:

$$\ln[S]_{SCSS} = \frac{14695}{T} - 9.656 + 1.02 \ln T + B' + \frac{CP}{T} + \sum_{M} X_M A_M /T \ + \ln a_{FeS}^{sulfide} - \ln a_{FeO}^{silicate} \quad (12)$$

In Equation (12) the only part of $\Delta G°$ which is treated as unknown is the pressure-dependence, with fit parameter C. The parameter B' in this case corresponds to A_0 of Equation (7)

Linear least-squares regression

We have a total of 392 experimental data (Table S1), 343 from previous studies and 49 from this work as the basis of our fits to Equations (11) and (12). These include data on hydrous melts containing up to 8.5 wt% H_2O equilibrated under conditions where the FeS-rich sulfide was a liquid. Note that we have explicit terms for the effect of H on $[S]_{SCSS}$ in our fits of equations (11) and (12) (Table 3). We started with the assumption that $a_{FeO}^{silicate}$ is equal to the mole fraction of FeO in the silicate melt on a single cation basis using components FeO, SiO_2, $AlO_{1.5}$ and so on. In practise, FeO

has an activity coefficient close to 1 in silicate melts over a fairly wide compositional range (Wood and Wade, 2013). The ideal approximation should, therefore, be adequate for our needs, particularly since any compositional dependence of $\gamma_{\mathrm{FeO}}^{silicate}$ will be absorbed by the A_{M} terms of Equations (11) and (12). An exception to this are experiments done at highly reducing conditions (i.e. below the iron-wüstite oxygen buffer). Silicate melts in equilibrium with sulfide melt under these conditions contain less than 1 wt% FeO. Based on sulfide/silicate trace element partitioning (Wood and Kiseeva, 2015) at these low FeO concentrations $\gamma_{\mathrm{FeO}}^{silicate}$ decreases by at least an order of magnitude and our assumption that $\gamma_{\mathrm{FeO}}^{silicate}$ is unity is no longer valid. To avoid these unusual compositions biasing our results we have therefore excluded from the regression six experiments with FeO_{Sil}/FeS_{Sul} ratios of less than 0.01. These are nevertheless shown in Figure 1 for comparison with the remaining 392 data.

Kiseeva and Wood (2013, 2015) have shown that, to a good approximation, sulfide liquids in igneous systems can be treated as ideal FeS-NiS-$CuS_{0.5}$ solutions when trace element partitioning between sulfide liquids and silicate melts is considered. We therefore began by approximating $a_{\mathrm{FeS}}^{sulfide}$ by $X_{\mathrm{FeS}}^{sulfide}$ where X is equal to Fe/(Fe+Ni+Cu). Following Kiseeva and Wood (2013) we took no explicit account of the presence of oxygen in the sulfide. Kiseeva and Wood (2013) found that the FeO content of the sulfide (in weight %) is approximately the same as the FeO content of the silicate in weight %. Nevertheless, they found that making explicit provision for the entropy of mixing of O^{2-} into the S^{2-} sublattice in FeS liquids using a Temkin-like solution model generated a worse approximation for $a_{\mathrm{FeS}}^{sulfide}$ than the simpler Fe/(Fe+Ni+Cu). We therefore began by using this simple "ideal" solution model.

Step-wise linear-regression of the dataset to equations (11) and (12) was carried out using the statistics package SPSS® with the requirement that fit parameters pass the F-test at F of 0.05. The results of the regression are presented in Table 3.

If we treat ΔG° and its temperature and pressure dependences as unknowns (Equation 11) then we find that $\Delta G^\circ/RT$ has a negative temperature-dependence which is compensated-for, as predicted, by negative values of almost all the A_M parameters. Thus, $[S]_{SCSS}$ increases with increasing temperature because the negative A_M/T terms become smaller with increasing temperature. Note that we tested the possibilities of adding cross-terms of the form $X_i X_j A_{ij}$ but found that only the $X_{Si}X_{Fe}$ term is significant. It is this term which controls the positive effect of FeO on S solubility. Note also that we have data for silicate melts containing between 0.3 and 40.1 weight% FeO, so the effect of FeO on S solubility is very well constrained.

Our second set of regressions assumed that ΔG° derived from thermodynamic data is correct and involved the fitting of Equation (12) to the same 392 data as before. In this case (Table 3) we have a slightly improved r^2 (0.977 instead of 0.963) and the negative A_M terms are all smaller than those obtained from the fit to Equation (11). This is because the temperature-dependence of ΔG° obtained from thermodynamic data is much less negative than that obtained by treating ΔH° and ΔS° as unknowns. Hence, the magnitudes of the negative terms required to compensate for the temperature dependence of ΔG° and to produce the observed positive temperature dependence of $[S]_{SCSS}$ are smaller if ΔG° is fixed at the tabulated value from thermodynamic data. As one might expect, the pressure term is, within uncertainty the same in both cases. Interestingly, the positive $X_{Si}X_{Fe}$ term is also the same in both cases within uncertainty. We consider therefore that this large positive cross-term is

well-constrained and realistic since it does not depend significantly on the assumptions made about the standard state free energy change of the sulfur dissolution reaction.

Figure 1 shows the results of the regression plotted as calculated $\ln[S]_{SCSS}$ versus the observed value for all 392 data used in the regression as well as the six experiments done under highly reducing conditions. 351 of 398 calculated $[S]_{SCSS}$ values fall within the range of 0.667-1.5 times the observed S concentrations, which we consider an excellent result considering the ranges of pressure (1 bar-24 GPa), temperature (1150-2160°C), FeO content of silicate (0.3-40.1%) sulfide composition covering the entire range of the FeS-NiS-$CuS_{0.5}$ system employed in the regression.

Effects of temperature, pressure and silicate melt composition

Figure 2a shows the effects of FeO content on S concentration at FeS saturation for melts ranging in composition from komatiitic to andesitic. Silicate melt compositions are given in Table 4. As anticipated from equation (6) calculated $[S]_{SCSS}$ is a u-shaped function of FeO content because of the trade-off between the positive coupling between S and FeO in the silicate and the negative influence of $a_{\mathrm{FeO}}^{silicate}$ on S solubility (O'Neill and Mavrogenes, 2002). Our model predicts that the solubility of S in silicate melts should reach a minimum at approximately 5 wt% FeO which is broadly consistent with the work of Li and Ripley (2005). The result disagrees, however, with the expressions of Holzheid and Grove (2002) and Fortin et al. (2015) which do not take account of the term in $a_{\mathrm{FeO}}^{silicate}$ required by Equation (6).

As can be seen in Figure 3a all compositions show a positive dependence of $[S]_{SCSS}$ on temperature. Note that results are, in some cases, extrapolated to temperatures below those of the silicate liquidi. Figure 3b shows a comparison of our results for $[S]_{SCSS}$ with literature models of S contents at FeS saturation for the MORB composition of Table 4. The latter are based on more limited datasets than that which was available to us. As can be seen, our results for MORB are in very good agreement with the model of Fortin et al. (2015) but that of Li and Ripley (2005) predicts much higher concentrations than those observed. The results of O'Neill and Mavrogenes (2002) are close to ours at their experimental temperature of 1400°C, but their equation does not provide for the correct form of the temperature extrapolation, as noted above.

Figures 4a, and 4b shows the calculated effects of pressure on the solubility of sulfur in the silicate melt compositions of Table 4 at a fixed temperature of 1400°C. All melts of concern exhibit predicted declines in $[S]_{SCSS}$ with increasing pressure, consistent with previously published results (Holzheid and Grove 2002). Figure 4b shows, consistent with Figure 3, that the best agreement with previous results is with the model of Fortin et al (2015).

Effect of sulfide composition

One of the major aims of our study was to investigate the effects of sulfide liquid composition on $[S]_{SCSS}$. As can be seen from Figure 1, and Table 2 the assumption of ideal FeS-NiS-$CuS_{0.5}$ solution produces very good fits to the experimental data over most of the composition range investigated and implies that $[S]_{SCSS}$ declines almost

linearly as Fe/(Fe+Ni+Cu) declines. It is known, however, that neither FeS-NiS (Fleet, 1989) nor FeS-$CuS_{0.5}$ (Eric and Timucin 1981) melt solutions are perfectly ideal and these deviations from ideality likely cause the deviations of $[S]_{SCSS}$ from the predicted values at low Fe/(Fe+Ni+Cu) (Table 2).

Nonideality in the sulfide solution can be treated in a number of different possible ways. We could use previously measured activity coefficients from the studies mentioned above. This would require re-fitting Equations (11) and (12) to derive new values of the A_M parameters. Since, however, our results indicate relatively small deviations from FeS-NiS-$CuS_{0.5}$ ideality, we have opted to use a simple non-ideal solution model and to treat the nonideality parameters as unknowns. In that case, applying a ternary symmetrical solution model for $a_{\mathrm{FeS}}^{sulfide}$ (e.g. Wood and Fraser, 1976) we add compositional terms as follows to that involving $X_{\mathrm{FeS}}^{sulfide}$

$$\ln a_{\mathrm{FeS}}^{sulfide} = \ln X_{\mathrm{FeS}}^{sulfide} + \frac{W_{\mathrm{NiFe}}}{RT} X_{\mathrm{NiS}}{}^{2} + \frac{W_{\mathrm{CuFe}}}{RT} X_{\mathrm{CuS_{0.5}}}{}^{2} + \frac{X_{\mathrm{NiS}} X_{\mathrm{CuS_{0.5}}}}{RT} (W_{\mathrm{NiFe}} + W_{\mathrm{CuFe}} - W_{\mathrm{NiCu}}) \quad (13)$$

In Equation (12) the W_{ij} parameters are the interaction parameters for i-j pairs and are obviously 0 if the solution is ideal. Treating the W_{ij}/R as fit parameters and adding them to Equation (12) yields:

$$\ln[\mathrm{S}]_{\mathrm{SCSS}} = \frac{14695}{T} - 9.656 + 1.02 ln T + B' + \frac{CP}{T} + \sum_{\mathrm{M}} X_{\mathrm{M}} A_{\mathrm{M}} / T + \ln X_{\mathrm{FeS}}^{sulfide}$$
$$+ \frac{D}{T}\left(X_{\mathrm{NiS}}{}^{2} + X_{\mathrm{NiS}} X_{\mathrm{CuS_{0.5}}}\right) + \frac{E}{T}\left(X_{\mathrm{CuS_{0.5}}}{}^{2} + X_{\mathrm{NiS}} X_{\mathrm{CuS_{0.5}}}\right)$$
$$+ \frac{F}{T}\left(-X_{\mathrm{NiS}} X_{\mathrm{CuS_{0.5}}}\right) - \ln a_{\mathrm{FeO}}^{silicate} \qquad (14)$$

We fitted Equation (13) to the same 392 $[S]_{SCSS}$ data as those used previously using, once more, stepwise linear regression. This approach led to *D* and *F* parameters which are not statistically significant and an *E* parameter of 546 K (Table 2). The latter reflects Fe-Cu interactions and its inclusion leads to improvements in calculated $[S]_{SCSS}$ for sulfur-rich compositions (Table 2). The overall improvement in r^2 is, however, very small, increasing from 0.977 to 0.978. An important point to note is that the fitted compositional A_M parameters (Table 2) are identical within uncertainty to those derived by assuming ideal sulfide solution.

Figures 5a, and 5b shows the calculated $[S]_{SCSS}$ for the MORB composition of Table 4 at saturation in FeS-NiS-$CuS_{0.5}$ sulfide of the indicated composition. In the ideal solution case of Figure 5a, sulfur solubility declines linearly at fixed ratio to X_{FeS} as discussed above. The non-ideal case of Figure 5b shows little difference from the ideal solution calculation at X_{FeS}>0.5, but differences between the two increase with decreasing X_{FeS}. At present we consider that the ideal solution model of Table 3 and Figure 5a is adequate for most geologic situations and certainly in those cases of X_{FeS}>0.5. The important point which we wish to reiterate is that $[S]_{SCSS}$ is extremely dependent on sulfide composition and should not be treated as a constant at fixed *P*, *T* and silicate composition. Supplement 2 comprises a spreadsheet for calculation of $[S]_{SCSS}$ using our regressed parameters for both ideal and non-ideal assumptions.

Application to natural systems

Based on Fe^{2+}/Fe^{3+} measurements the fO_2 of MORB has been estimated to be around that of the fayalite-magnetite-quartz (FMQ) oxygen buffer (Cottrell and Kelley, 2013). Under these conditions sulfur will be present dominantly as S^{2-}, suggesting that the Fincham - Richardson relationship should apply to MORB melts. Although chemical and textural evidence (Peach et al., 1990; Patten et el., 2013) suggests that MORBs are sulfide saturated throughout their crystallization histories, most previous models for SCSS, imply, in contrast, that MORBs are sulfide undersaturated during much of crystallization (O'Neill and Mavrogenes, 2002; Li and Ripley, 2005; Li and Ripley, 2009; Fortin et al., 2015) (Fig. 6a).

To address this apparent discrepancy, we have taken an average of primitive MORB glass compositions (MgO > 9.3 wt%) from Jenner and O'Neill (2012) and determined the liquid line of descent from 1230 to 1170°C using Petrolog3 (Danyushevsky and Plechov, 2011). We then applied our model for SCSS assuming ideal solution in the immiscible sulfide, a pressure of 0.3 GPa and a Fe/(Fe+Ni+Cu) of 0.7 common to sulfides found in MORB (Patten et al. 2013; Peach et al., 1990).

The results for SCSS along the liquid line of descent of MORB based on the model presented here agree with the high sulfur contents of MORB glasses measured by Jenner and O'Neill (2012) over the entire range of MgO contents. In contrast, as discussed above, most previous $[S]_{SCSS}$ expressions suggest that, over a significant range of MgO concentrations MORB melts are undersaturated with respect to S

(O'Neill and Mavrogenes, 2002; Li and Ripley, 2005; Li and Ripley, 2009; Fortin et al., 2015) as shown in Figure 6a. The two exceptions to this are the models of Mavrogenes and O'Neill (1999) and Holzheid and Grove (2002) which substantially underpredict the S contents of the MORB glasses. Although there is a pronounced cluster of S analyses along our predicted trend at sulfide saturation (Fig. 6) we note that a number of S concentrations fall below those we calculate. Lower sulfur concentrations are plausibly the result of degassing of the melt during eruption (Fig. 6b). We therefore conclude, based on our measurements that the MORB source region is sulfide saturated and the melts remain at sulfide saturation throughout their crystallization histories.

Implications and conclusions

We have demonstrated that the solubility of sulfur in silicate melt at sulfide saturation $[S]_{SCSS}$ depends, at fixed pressure, temperature and silicate melt composition, on the composition of the sulfide liquid. This dependence, to a good approximation, leads to $[S]_{SCSS}$ being a linear function of the mole fraction of FeS in the sulfide liquid, defined as ($X_{\mathrm{FeS}}^{sulfide}$ = Fe/(Fe+Ni+Cu)). Departures from linear behavior at $X_{\mathrm{FeS}}^{sulfide}$ below ~0.5 are consistent with known non-idealities in the FeS-NiS and FeS-$CuS_{0.5}$ liquid systems.

We took both ideal and non-ideal sulfide solution models and fit $[S]_{SCSS}$ to the available data using and equation of similar form to that of O'Neill and Mavrogenes (2002):

$$\ln[\mathrm{S}]_{\mathrm{SCSS}} = \frac{\Delta G^{\circ}}{RT} + A_0 + \sum_{\mathrm{M}} X_{\mathrm{M}} A_{\mathrm{M}} / T \; + \ln a_{\mathrm{FeS}}^{sulfide} - \ln a_{\mathrm{FeO}}^{silicate}$$

470

471 In this equation ΔG° is the standard state free energy change for the reaction:

472

$$\mathrm{FeO}^{silicate} + \frac{1}{2}\mathrm{S}_2 = \mathrm{FeS}^{sulfide} + \frac{1}{2}\mathrm{O}_2$$

473

474 The expression for $[\mathrm{S}]_{\mathrm{SCSS}}$ incorporates compositional parameters A_{M} in terms
475 dependent on X_{M} the mole fraction of the oxide of M in the silicate melt on a single
476 cation basis. The activities $a_{\mathrm{FeO}}^{solicate}$ and $a_{\mathrm{FeS}}^{sulfide}$ were assumed equal to the mole
477 fractions of FeO in the silicate and FeS in the sulfide respectively except where the
478 latter was treated as a (nonideal) ternary symmetrical solution.

479

480 We fitted $[\mathrm{S}]_{\mathrm{SCSS}}$ to the 392 available data points in order to derive best-fit values of
481 A_0 and the A_{M} together with the pressure-dependence of ΔG°.The standard free energy
482 change ΔG° was adopted from O'Neill and Mavrogenes (2002). Since $[\mathrm{S}]_{\mathrm{SCSS}}$ is
483 observed to have a positive dependence on temperature while ΔG° *decreases* with
484 increasing temperature, the A_{M} parameters are required to be mostly negative. We
485 tested this conclusion by treating ΔG° and its temperature dependence ΔS° as
486 unknowns and fitted Equation (11), which has these extra unknowns, to the data. As
487 before, the best-fit ΔG° has a negative temperature-dependence and the fit parameters
488 are all negative except for a cross-term A_{SiFe} which takes account of a positive
489 correlations between $[\mathrm{S}]_{\mathrm{SCSS}}$ and the product $X_{\mathrm{Si}}X_{\mathrm{Fe}}$.

490

We find that the cross-term A_{SiFe} is extremely robust in that it has, within uncertainty, the same value (~113000K) in all 3 cases considered (a) ΔG° treated as a *P-T* dependent fit parameter, with ideal FeS-NiS-$CuS_{0.5}$ sulfide solution (b) ΔG° at 1 bar adopted from thermodynamic data and assuming ideal FeS-NiS-$CuS_{0.5}$ sulfide solution and (c) ΔG° at 1 bar adopted from thermodynamic data and assuming nonideal FeS-NiS-$CuS_{0.5}$ sulfide solution.

The large positive term in $X_{Si}X_{Fe}$ (on a single cation basis) means that $[S]_{SCSS}$ is predominantly dependent on the FeO content of the silicate melt decreasing (for FeS saturation at 1 GPa, 1400°C) from 4692 ppm for a Martian basalt with 17.9 wt% FeO to 1084 ppm for Andesite with 7.7 wt% FeO.

In agreement with previous versions of the effects of pressure and temperature on $[S]_{SCSS}$, all natural silicate melt compositions considered exhibit positive dependences on temperature and negative dependences of $[S]_{SCSS}$ on pressure. Our results are, however, in best agreement with those of Fortin et al (2015).

Finally, application of our results to the MORB glasses analysed by Jenner and O'Neill (2012) indicates that MORB are sulfide saturated throughout their crystallisation paths.

Acknowledgements

We would like to thank Roman Botcharnikov and John Mavrogenes for their thoughtful reviews and Don Baker for editorial handling. This work was funded by

European Research Council grant 267764 to BJW and by NERC grant NE/L010828/1 to ESK.

References

Ariskin A.A., Danyushevsky L.V., Bychkov K.A. McNeill, A.W. Barmina, G.S., and Nikolaev, G.S. (2013) Modeling Solubility of Fe-Ni Sulfides in Basaltic Magmas: The Effect of Nickel. Economic Geology 108, 1983-2003.

Bridges J.C. and Warren P.H. (2006) The SNC meteorites: basaltic igneous processes on Mars. Journal of the Geological Society 163, 229–251.

Cottrell E., and Kelley K.A. (2013) Redox heterogeneity in mid-ocean ridge basalts as a function of mantle source. Science 340, 1314–7.

Danyushevsky L.V., and Plechov P. (2011) Petrolog3: Integrated software for modeling crystallization processes. Geochemistry, Geophysics, Geosystems 12.

Eric H., and Timucin M. (1981) Activities in Cu_2S-FeS-PbS Melts at 1200°C. Metallurgical Transactions B 12, 493-500.

Fincham C.J.B., and Richardson F.D. (1954) The Behaviour of Sulphur in Silicate and Aluminate Melts. Proceedings of the Royal Society A: Mathematical, Physical and Engineering Sciences 223, 40–62.

Fischer T.P., Giggenbach W.F., Sano Y., and Williams S.N. (1998) Fluxes and

sources of volatiles discharged from kudryavy, a subduction zone volcano, Kurile Islands. Earth and Planetary Science Letters 160, 81–86.

Fleet M.E. (1989) Activity coefficients for FeS and NiS in monosulfide liquid and $NiSi_{1/2}O_2$ in olivine from sulfide-silicate equilibria. Geochimica et Cosmochimica Acta 53, 791–796.

Fortin M.-A., Riddle J., Desjardins-Langlais Y., and Baker D.R. (2015) The effect of water on the sulfur concentration at sulfide saturation (SCSS) in natural melts. Geochimica et Cosmochimica Acta 160, 100–116.

Francis R.D. (1990) Sulfide globules in mid-ocean ridge basalts (MORB), and the effect of oxygen abundance in Fe-S-O liquids on the ability of those liquids to partition metals from MORB and komatiite magmas. Chemical Geology 85, 199–213.

Gale A., Dalton C.A., Langmuir C.H., Su Y., and Schilling J.G. (2013) The mean composition of ocean ridge basalts. Geochemistry, Geophysics, Geosystems 14, 489–518.

Haughton D.R., Roeder P.L., and Skinner B.J. (1974) Solubility of sulfur in mafic magmas. Economic Geology 69, 451–467.

Holzheid A., and Grove T.L. (2002) Sulfur saturation limits in silicate melts and their implications for core formation scenarios for terrestrial planets. American

566 Mineralogist 87, 227–237.
567
568 Jenner F.E., and O'Neill H.S.C. (2012) Analysis of 60 elements in 616 ocean floor
569 basaltic glasses. Geochemistry, Geophysics, Geosystems 13, 1–11.
570
571 Katsura T., and Nagashima S. (1974) Solubility of sulfur in some magmas at 1
572 atmosphere. Geochimica et Cosmochimica Acta 38, 517–531.
573
574 Kiseeva E.S., and Wood B.J. (2013) A simple model for chalcophile element
575 partitioning between sulphide and silicate liquids with geochemical applications.
576 Earth and Planetary Science Letters 383, 68–81.
577
578 Kiseeva E.S., and Wood B.J. (2015) The effects of composition and temperature on
579 chalcophile and lithophile element partitioning into magmatic sulphides. Earth
580 and Planetary Science Letters 424, 280–294.
581
582 Li C., and Ripley E.M. (2005) Empirical equations to predict the sulfur content of
583 mafic magmas at sulfide saturation and applications to magmatic sulfide
584 deposits. Mineralium Deposita 40, 218–230.
585
586 Li C., and Ripley E.M. (2009) Sulfur contents at sulfide-liquid or anhydrite saturation
587 in silicate melts:Empirical equations and example applications. Economic
588 Geology 104, 405–412.
589
590 Liu Y., Samaha N.-T., and Baker D.R. (2007) Sulfur concentration at sulfide

saturation (SCSS) in magmatic silicate melts. Geochimica et Cosmochimica Acta 71, 1783–1799.

Mavrogenes J.A., and O'Neill H.S.C. (1999) The relative effects of pressure, temperature and oxygen fugacity on the solubility of sulfide in mafic magmas. Geochimica et Cosmochimica Acta 63, 1173–1180.

Mungall J.E. (2007) Magmatic ore deposits. In Treatise on Geochemistry Elsevier Ltd. pp. 1–33.

O'Neill H.S.C., and Mavrogenes J.A. (2002) The Sulfide Capacity and the Sulfur Content at Sulfide Saturation of Silicate Melts at 1400°C and 1 bar. Journal of Petrology 43, 1049–1087.

Parman S.W., Shimizu N., Grove T.L. and Dann J.C. (2003) Constraints on the pre-metamorphic trace element composition of Barberton komatiites from ion probe analyses of preserved clinopyroxene. Contributions to Mineralogy and Petrology 144, 383–396.

Patten C., Barnes S.J., Mathez E.A., and Jenner F.E. (2013) Partition coefficients of chalcophile elements between sulfide and silicate melts and the early crystallization history of sulfide liquid: LA-ICP-MS analysis of MORB sulfide droplets. Chemical Geology 358, 170–188.

Peach C.L., Mathez E.A., and Keays R.R. (1990) Sulfide melt-silicate melt

distribution coefficients for noble metals and other chalcophile elements as deduced from MORB: Implications for partial melting. Geochimica et Cosmochimica Acta 54, 3379–3389.

Presnall D.C., Dixon S.A., Dixon J.R., O'Donnell T.H., Brenner N.L., Schrock R.L., and Dycus D.W. (1978) Liquidus phase relations on the join diopside-forsterite-anorthite from 1 atm to 20 kbar: Their bearing on the generation and crystallization of basaltic magma. Contributions to Mineralogy and Petrology 66, 203–220.

Shima H., and Naldrett A.J. (1975) Solubility of sulfur in an ultramafic melt and the relevance of the system Fe-S-O. Economic Geology 70, 960–967.

Tuff J., Wood B.J., and Wade J. (2011) The effect of Si on metal-silicate partitioning of siderophile elements and implications for the conditions of core formation. Geochimica et Cosmochimica Acta 75, 673-690.

Wallace P.J. (2005) Volatiles in subduction zone magmas: Concentrations and fluxes based on melt inclusion and volcanic gas data. Journal of Volcanology and Geothermal Research 140, 217–240.

Wallace P.J., and Carmichael I.S.E. (1992) Sulfur in basaltic magmas. Geochimica et Cosmochimica Acta 56, 1863-1874.

Wilkinson J.F.G. (1986) Classification and average chemical compositions of

common basalts and andesites. Journal of Petrology 27, 31–62.

Wood B.J., and Fraser D.G. (1976) Elementary Thermodynamics for Geologists. Oxford University Press, Oxford, U.K.

Wood B.J., Kiseeva E.S., and Mirolo F.J. (2014) Accretion and core formation: the effects of sulfur on metal-silicate partition coefficients. Geochimica et Cosmochimica Acta 145, 248–267.

Wood B.J., and Kiseeva E.S. (2015) Trace element partitioning into sulfide: How lithophile elements become chalcophile and vice versa. American Mineralogist 100, 2371-2379.

Wood B.J., and Wade J. (2013) Activities and volatilities of trace components in silicate melts: A novel use of metal-silicate partitioning data. Contributions to Mineralogy and Petrology 166, 911–921.

Figure captions

Figure 1. Observed values of SCSS vs. calculated using coefficients for the ideal sulfide melt solution model (Table 3) for 398 synthetic silicate melts equilibrated with immiscible sulfide melt (Table S1). Red diamonds represent experiments done at highly reducing conditions which were not included in the regression (see text).

Figure 2. Compositional dependence of SCSS at 1 GPa assuming an immiscible sulfide liquid of pure FeS for (a) four different melt compositions with varying FeO concentrations using the model presented in this study and (b) for MORB comparing predicted SCSS from the present study to those from previous investigations (Holzheid and Grove, 2002; Li and Ripley, 2005; Fortin et al., 2015).

Figure 3. Temperature dependence of SCSS at 1 GPa assuming an immiscible sulfide liquid of pure FeS for (a) different melt compositions using the model presented in this study and (b) for MORB comparing predicted SCSS from the present study to those from previous investigations (Mavrogenes and O'Neill, 1999; Holzheid and Grove, 2002; Li and Ripley, 2005; Fortin et al., 2015).

Figure 4. Pressure dependence of SCSS at 1400°C assuming an immiscible sulfide liquid of pure FeS for (a) different melt compositions using the model presented in this study and (b) for MORB comparing predicted SCSS from the present study to those from previous investigations (Holzheid and Grove, 2002; Li and Ripley, 2005; Fortin et al., 2015).

Figure 5. Ternary plots showing predicted SCSS in average MORB at 1400°C and 1 GPa assuming (a) ideal, and (b) nonideal solution models for sulfide melt. Numbers represent the S concentration in the silicate melt in ppm, orange squares are the sulfide melt compositions presented in this study and grey diamonds are those of previous investigations (Table S1).

691

692 **Figure 6.** (a) Sulfur contents of MORB glasses as a function of wt% MgO measured
693 by Jenner and O'Neill (2012) compared to predicted values of SCSS from this
694 and previous studies along the MORB liquid line of descent (Mavrogenes and
695 O'Neill, 1999; Holzheid and Grove, 2002; O'Neill and Mavrogenes, 2002; Li
696 and Ripley, 2005; Li and Ripley, 2009; Fortin et al., 2015). (b) Comparison of
697 sulfur contents of MORB glasses to values of SCSS predicted by this study and
698 the expected effects of magma degassing.

699

Table 1. Experimental run conditions

Sample	Starting composition	Temperature (°C)	Pressure (GPa)	Capsule	Duration (min)
Ni2-1	$An_{50}Di_{28}Fo_{22}$ + 5%FeO + 25%FeS + 25%NiS	1400	1.5	Graphite	120
Cu6-2	Basalt + 6%FeO + 42%FeS + 8%Cu_2S	1400	1.5	SiO_2	120
Ni2-2	$An_{50}Di_{28}Fo_{22}$ + 5%FeO + 25%FeS + 25%NiS	1400	1.5	SiO_2	90
Ni3-2	$An_{50}Di_{28}Fo_{22}$ + 5%FeO + 25%FeS + 25%Ni_3S_2	1400	1.5	SiO_2	120
Ni4-1	$An_{50}Di_{28}Fo_{22}$ + 5%FeO + 10%FeS + 20%Ni_3S_2 + 20%Cu_2S	1400	1.5	SiO_2	120
Ni5-1	Basalt + 25%Ni_3S_2 + 25%Cu_2S	1400	1.5	SiO_2	135
F1-1	$An_{42}Di_{58}$ + 10%FeO + 50%FeS	1650	1.5	Graphite	40
F2-1	$An_{28}Di_{39}Qz_{33}$ + 10%FeO + 50%FeS	1650	1.5	Graphite	30
F3-1	$An_{17}Di_{23}Wo_{60}$ + 10%FeO + 50%FeS	1650	1.5	Graphite	30
F4-1	$Wo_{67}Qz_{33}$+ 10%FeO + 50%FeS	1650	1.5	Graphite	30
F5-1	$An_{50}Di_{28}Fo_{22}$ + 10%FeO + 50%FeS	1650	1.5	Graphite	30
F6-1	$An_{41}Di_{23}Fo_{41}Per_{18}$ + 10%FeO + 50%FeS	1650	1.5	Graphite	30
F7-1	$An_{35}Di_{19}Fo_{15}Qz_{31}$ + 10%FeO + 50%FeS	1650	1.5	Graphite	35
F8-1	$Fo_{61}Qz_{39}$ + 10%FeO + 50%FeS	1650	1.5	Graphite	30
F9-1	$An_{95}Cor_5$ + 10%FeO + 50%FeS	1650	1.5	Graphite	40
F10-1	$Fo_{50}And_{19}Qz_{31}$ + 10%FeO + 50%FeS	1650	1.5	Graphite	30
F11-1	$An_{81}Per_{15}And_4$ + 10%FeO + 50%FeS	1650	1.5	Graphite	30
KK9-3	$An_{50}Di_{28}Fo_{22}$ + 10%FeO + 45%FeS +5%NiS	1400	1.5	Pt-Graphite	180
KK10-2	Haplobasalt + 10%FeO + 48%FeS +2%NiS	1400	1.5	Pt-Graphite	60
KK10-5	Haplobasalt + 10%FeO + 48%FeS +2%NiS	1400	1.5	Graphite	1080
KK14-1	Basalt + 6%FeO + 49.5%FeS + 0.5%NiS	1400	1.5	Pt-Graphite	120
KK14-2	Basalt + 6%FeO + 49.5%FeS + 0.5%NiS	1400	1.5	Pt-Graphite	90
KK25-1	Andesite + 48%FeS +2%NiS	1400	1.5	Graphite	120
KK26-1	Dacite + 48%FeS +2%NiS	1400	1.5	Graphite	165
KK30-1	BCR-2 + 15%$Ab_{33}Or_{50}Fo_{17}$ + 49%FeS + 1% NiS	1400	1.5	Graphite	135
KK31-1	Phonolite + 48%FeS +1%NiS + 1%Cu_2S	1400	1.5	Graphite	120
KK32-1	$Ab_{79}Fo_{21}$ + 2.5%FeO + 45%FeS + 2.5%NiS + 2.5%Cu_2S	1400	1.5	Graphite	135
KK37-1	Diabase + 45%FeS + 2.5%NiS + 2.5% Cu_2S	1635	1.5	Graphite	30
A717	$An_{50}Di_{28}Fo_{22}$ + 50%FeS	1800	2.5	Graphite	20
A716	$An_{50}Di_{28}Fo_{22}$ + 10%FeO + 50%FeS	1800	2.5	Graphite	20
A718	$An_{50}Di_{28}Fo_{22}$ + 20%FeO + 50%FeS	1800	2.5	Graphite	20
B283	$An_{50}Di_{28}Fo_{22}$ + 50%Cu_2S	1525	1.5	Pt-Graphite	140
B284	$An_{50}Di_{28}Fo_{22}$ + 50%NiS	1525	1.5	Pt-Graphite	60
B285	$An_{50}Di_{28}Fo_{22}$ + 50%FeS	1800	1.5	Graphite	20
B286	$An_{50}Di_{28}Fo_{22}$ + 10%FeO + 50%FeS	1800	1.5	Graphite	20
B287	$An_{50}Di_{28}Fo_{22}$ + 20%FeO + 50%FeS	1800	1.5	Graphite	30
C138	Basalt + 50%FeO + 50%FeS	1800	5.5	Graphite	15
C140	$An_{50}Di_{28}Fo_{22}$ + 50%FeS	1800	5.5	Graphite	10
C141	$An_{50}Di_{28}Fo_{22}$ + 50%FeS	1800	5.5	Graphite	10
C142	$An_{50}Di_{28}Fo_{22}$ + 10%FeO + 50%FeS	1800	5.5	Graphite	10
C143	$An_{50}Di_{28}Fo_{22}$ + 20%FeO + 50%FeS	1800	5.5	Graphite	10
B291	$An_{50}Di_{28}Fo_{22}$ + 10%FeO + 50%NiS	1500	1.5	Graphite	60
B292	$An_{50}Di_{28}Fo_{22}$ + 10%FeO + 50%Cu_2S	1500	1.5	Graphite	60
B293	$An_{50}Di_{28}Fo_{22}$ + 10%FeO + 25%NiS + 25%Cu_2S	1500	1.5	Graphite	60
735	$Di_{61}An_{10}Qz_{29}$ + 25%FeO + 50%FeS	1800	7	Graphite	10
753	Peridotite + 5%SiO_2 +50%FeS	2160	24	MgO	10
1605	$An_{50}Di_{28}Fo_{22}$ + 15%FeO + 33%FeS + 33%NiS + 33%Cu_2S	1600	1.5	Graphite	20
1606	$An_{50}Di_{28}Fo_{22}$ + 10%FeO + 33%FeS + 33%NiS + 33%Cu_2S	1600	1.5	Graphite	20
1607	$An_{50}Di_{28}Fo_{22}$ + 20%FeO + 33%FeS + 33%NiS + 33%Cu_2S	1600	1.5	Graphite	20

An - anorthite, Di - diopside, Fo - forserite, Qz - quartz, Wo - wollastonite, Per - periclase, Cor - corundum, And - andalusite, BCR-2 - USGS Columbia River Basalt

Table 2. Compositions of silicate glass and sulfide in wt% measured by EPMA

Sample	Ni2-1	Cu6-2	Ni2-2	Ni3-2	Ni4-1	Ni5-1	F1-1	F2-1	F3-1	F4-1
SiO_2	44.23 (0.06)	54.83 (0.55)	57.16 (0.19)	58.62 (0.27)	55.86 (0.17)	62.91 (0.51)	43.31 (0.39)	54.44 (0.23)	43.93 (0.32)	55.51 (0.94)
TiO_2	0.01 (0.01)	0.40 (0.01)				0.64 (0.03)				
Al_2O_3	17.71 (0.06)	7.78 (0.17)	12.05 (0.14)	11.27 (0.58)	9.52 (0.09)	12.25 (0.10)	13.56 (0.11)	13.22 (0.09)	5.44 (0.06)	0.14 (0.02)
FeO	0.88 (0.03)	5.07 (0.12)	5.56 (0.09)	4.58 (0.16)	4.13 (0.06)	2.74 (0.05)	10.76 (0.55)	12.85 (0.17)	10.38 (0.46)	13.25 (0.68)
MgO	17.70 (0.13)	12.93 (0.38)	10.55 (0.09)	11.62 (0.26)	10.77 (0.06)	8.63 (0.15)	9.33 (0.07)	4.58 (0.03)	4.07 (0.04)	0.13 (0.02)
CaO	16.44 (0.09)	15.33 (0.09)	12.11 (0.09)	11.99 (0.17)	15.98 (0.07)	10.38 (0.13)	20.12 (0.18)	13.07 (0.08)	32.67 (0.25)	27.05 (0.47)
MnO	0.01 (0.01)	0.07 (0.01)	0.02 (0.02)	0.04 (0.01)	0.01 (0.01)	0.16 (0.01)				
Na_2O	0.35 (0.01)	0.33 (0.02)				1.30 (0.03)				
K_2O	0.01 (0.01)	0.11 (0.01)				0.12 (0.01)				
P_2O_5		0.14 (0.01)				0.04 (0.01)				
S (ppm)	4970 (90)	1443 (436)	2179 (86)	618 (57)	325 (45)	159 (62)	5789 (2755)	4921 (1033)	7993 (2252)	8411 (3420)
Total	97.83	97.00	97.67	98.17	96.31	99.14	97.66	98.65	97.29	96.93
Fe	44.91 (0.39)	52.04 (7.43)	42.98 (1.38)	31.39 (6.67)	13.40 (6.75)	5.69 (0.51)	59.37 (0.69)	59.03 (1.47)	59.91 (0.85)	59.04 (0.72)
Ni	14.98 (0.17)	0.36 (0.09)	15.90 (0.97)	35.26 (8.72)	34.00 (19.97)	28.20 (7.53)	0.62 (0.08)	1.11 (0.33)	0.89 (0.38)	0.79 (0.04)
Cu	0.31 (0.05)	11.07 (8.42)	0.23 (0.10)	0.73 (0.40)	24.28 (26.8)	29.53 (8.18)	1.01 (0.20)	1.30 (0.18)	0.61 (0.11)	1.10 (0.15)
S	37.46 (0.57)	33.31 (2.23)	33.41 (0.92)	31.72 (2.62)	35.97 (3.60)	36.49 (0.86)	36.60 (0.85)	34.73 (2.38)	32.74 (1.81)	37.52 (0.64)
O	0.09 (0.07)	0.56 (0.45)	0.22 (0.09)	0.42 (0.21)	0.26 (0.21)	n.d.	1.48 (0.65)	2.66 (1.64)	2.11 (1.21)	1.32 (0.45)
Total	97.75	97.34	92.75	99.53	107.91	99.90	99.08	98.83	96.27	99.76
S (calc.)[a]	7031 (1921)	1481 (405)	904 (247)	569 (155)	320 (87)	80 (22)	4267 (1166)	3444 (941)	7978 (2179)	9298 (2540)
S (calc.)[b]	6545 (1749)	1423 (380)	870 (232)	547 (146)	329 (88)	90 (24)	4181 (1118)	3499 (935)	7578 (2026)	9164 (2449)
Sample	F5-1	F6-1	F7-1	F8-1	F9-1	F10-1	F11-1	KK9-3	KK10-2	KK10-5
SiO_2	41.08 (0.23)	34.72 (0.80)	52.69 (0.18)	54.40 (0.39)	37.39 (0.15)	50.27 (0.43)	36.10 (0.29)	41.46 (0.10)	52.03 (0.16)	52.19 (0.62)
TiO_2										0.02 (0.01)
Al_2O_3	16.63 (0.10)	13.82 (1.17)	10.49 (0.06)	0.21 (0.03)	34.04 (0.10)	10.65 (0.10)	25.55 (0.32)	16.47 (0.06)	15.60 (0.02)	15.33 (0.18)
FeO	9.13 (0.34)	8.70 (0.43)	13.56 (0.22)	14.23 (0.48)	11.60 (0.19)	12.67 (0.30)	9.74 (0.22)	7.19 (0.08)	9.17 (0.09)	10.05 (0.13)
MgO	15.37 (0.07)	26.87 (2.29)	10.25 (0.07)	29.21 (0.77)	0.21 (0.02)	23.97 (0.15)	11.65 (0.15)	14.98 (0.05)	8.98 (0.07)	8.92 (0.07)
CaO	15.29 (0.17)	14.26 (1.67)	10.13 (0.07)	0.42 (0.06)	16.64 (0.09)	0.35 (0.01)	15.83 (0.16)	15.12 (0.08)	10.60 (0.08)	10.97 (0.08)
MnO										0.05 (0.01)
Na_2O										0.07 (0.01)
K_2O										
P_2O_5										
S (ppm)	4563 (1372)	4845 (1827)	4358 (1027)	4249 (990)	2942 (529)	4041 (1292)	3806 (838)	2402 (114)	2165 (129)	1644 (95)
Total	97.96	98.86	97.56	98.90	100.18	98.32	99.26	95.46	96.59	97.77
Fe	59.78 (0.80)	59.59 (0.92)	58.59 (0.98)	58.39 (0.99)	59.22 (1.24)	56.89 (0.86)	60.08 (0.76)	57.71 (0.64)	61.41 (0.44)	61.41 (0.59)
Ni	0.28 (0.03)	1.10 (0.32)	1.61 (0.36)	1.07 (0.16)	2.22 (0.51)	1.72 (0.12)	0.72 (0.16)	2.93 (0.06)	0.92 (0.11)	1.56 (0.05)
Cu	1.12 (0.19)	0.93 (0.18)	1.11 (0.23)	1.15 (0.23)	0.93 (0.21)	1.30 (0.29)	0.75 (0.11)	n.d	n.d	n.d
S	35.90 (0.71)	36.47 (1.78)	37.75 (0.89)	37.20 (1.01)	35.77 (1.51)	37.12 (0.91)	37.36 (1.33)	35.68 (0.42)	37.84 (0.16)	36.29 (0.55)
O	1.62 (0.56)	2.61 (1.07)	1.56 (0.65)	2.03 (0.83)	1.95 (0.95)	1.53 (0.71)	2.66 (1.03)	1.52 (0.31)	1.38 (0.11)	2.02 (0.44)
Total	98.70	100.70	100.63	99.85	100.10	98.56	101.57	97.84	101.55	101.27
S (calc.)[a]	3593 (982)	4762 (1301)	3525 (963)	3309 (904)	2430 (664)	2354 (643)	3285 (897)	2326 (635)	1495 (408)	1630 (445)
S (calc.)[b]	3542 (947)	4672 (1249)	3603 (963)	3454 (923)	2386 (638)	2439 (652)	3219 (861)	2193 (586)	1452 (388)	1585 (424)

(continued on next page)

700

Sample	KK14-1	KK14-2	KK25-1	KK26-1	KK30-1	KK31-1	KK32-1	KK37-1	A717	A716
SiO_2	47.52 (0.17)	48.23 (0.31)	60.64 (0.29)	56.28 (1.66)	54.45 (0.87)	52.84 (0.21)	57.32 (0.23)	49.50 (0.18)	47.09 (0.18)	44.70 (0.22)
TiO_2	0.78 (0.02)		0.56 (0.02)	0.34 (0.02)	1.39 (0.06)	1.48 (0.03)	0.02 (0.01)	0.87 (0.02)	0.01 (0.01)	0.03 (0.01)
Al_2O_3	14.89 (0.08)	15.00 (0.17)	16.75 (0.07)	15.76 (0.39)	13.96 (0.59)	18.80 (0.10)	14.39 (0.08)	9.39 (0.09)	9.97 (0.06)	10.08 (0.07)
FeO	9.06 (0.12)	8.28 (0.32)	5.47 (0.08)	5.16 (0.40)	7.10 (0.14)	4.43 (0.06)	7.05 (0.05)	11.23 (0.25)	3.12 (0.34)	7.59 (0.08)
MgO	9.99 (0.06)	10.06 (0.13)	3.15 (0.13)	3.34 (0.44)	5.39 (0.33)	3.70 (0.08)	10.36 (0.09)	16.94 (0.11)	21.34 (0.09)	20.04 (0.09)
CaO	11.89 (0.05)	11.99 (0.10)	5.98 (0.05)	11.35 (1.09)	6.74 (0.38)	4.42 (0.06)	0.66 (0.03)	7.80 (0.05)	18.17 (0.26)	16.81 (0.11)
MnO	0.13 (0.02)		0.09 (0.01)	0.07 (0.02)	0.10 (0.02)	0.03 (0.02)	0.04 (0.01)	0.04 (0.02)		
Na_2O	1.76 (0.02)	1.80 (0.03)	3.74 (0.05)	2.62 (0.06)	3.31 (0.06)	7.96 (0.15)	7.58 (0.08)	1.22 (0.09)	0.05 (0.01)	0.04 (0.02)
K_2O			1.14 (0.02)	2.50 (0.24)	3.20 (0.08)	3.29 (0.05)	0.03 (0.01)	0.74 (0.03)		
P_2O_5				n.d	0.09 (0.01)	n.d	n.d	0.02 (0.01)		
S (ppm)	2348 (108)	2343 (118)	885 (79)	1210 (244)	744 (106)	712 (41)	644 (41)	2732 (579)	5696 (1388)	3358 (391)
Total	96.25	95.60	97.62	97.54	95.72	97.01	97.52	98.00	100.33	99.63
Fe	60.79 (0.91)	60.76 (0.72)	56.96 (0.64)	61.92 (0.41)	59.79 (0.56)	58.49 (1.33)	57.83 (0.81)	57.98 (1.85)	64.66 (0.30)	63.74 (0.22)
Ni	0.34 (0.03)	0.26 (0.03)	1.34 (0.06)	0.23 (0.05)	0.80 (0.04)	1.20 (0.06)	2.18 (0.04)	1.46 (0.13)	0.06 (0.03)	0.05 (0.02)
Cu	n.d	n.d	1.28 (0.13)	0.15 (0.03)	0.89 (0.09)	0.86 (0.14)	1.22 (0.19)	3.66 (1.84)	0.08 (0.04)	0.11 (0.02)
S	36.32 (0.71)	36.04 (0.69)	35.02 (0.70)	36.95 (0.60)	37.08 (0.75)	38.19 (0.91)	35.57 (0.52)	36.38 (1.59)	34.27 (0.58)	35.54 (0.45)
O	1.92 (0.53)	2.05 (0.22)	1.70 (0.69)	0.63 (0.35)	2.14 (0.76)	2.66 (0.73)	2.11 (0.38)	2.33 (1.5)	1.67 (0.55)	0.42 (0.26)
Total	99.37	99.11	96.29	99.87	100.70	101.40	98.92	101.81	100.73	99.86
S (calc.)[a]	1918 (524)	1779 (486)	639 (175)	864 (236)	800 (219)	819 (224)	912 (249)	2623 (717)	7127 (1947)	4639 (1267)
S (calc.)[b]	1855 (496)	1712 (458)	636 (170)	849 (227)	809 (216)	826 (221)	912 (244)	2686 (718)	7105 (1899)	4663 (1246)

Sample	A718	B283	B284	B285	B286	B287	C138	C140	C141	C142
SiO_2	43.49 (0.27)	47.51 (0.26)	47.60 (0.14)	47.50 (0.64)	45.33 (0.26)	43.58 (0.27)	49.72 (0.11)	47.30 (0.22)	47.18 (0.42)	43.70 (0.14)
TiO_2	0.01 (0.01)	0.02 (0.01)	0.02 (0.01)	0.05 (0.01)	0.03 (0.01)	0.03 (0.01)	0.77 (0.05)	0.03 (0.01)	0.01 (0.01)	0.03 (0.01)
Al_2O_3	9.42 (0.06)	17.03 (0.15)	16.44 (0.04)	10.05 (0.03)	9.41 (0.07)	8.99 (0.11)	13.40 (0.10)	9.60 (0.17)	10.15 (0.13)	9.59 (0.07)
FeO	10.07 (0.42)	0.01 (0.01)	0.00 (0.01)	3.27 (0.26)	7.24 (0.26)	10.45 (0.25)	7.51 (0.16)	3.37 (0.09)	2.11 (0.22)	8.46 (0.11)
MgO	19.61 (0.22)	12.89 (0.05)	13.32 (0.05)	21.33 (0.04)	20.39 (0.09)	19.78 (0.08)	11.16 (0.11)	19.97 (0.24)	21.99 (0.40)	20.33 (0.07)
CaO	16.76 (0.14)	20.28 (0.18)	20.56 (0.17)	17.65 (0.1)	17.20 (0.27)	16.40 (0.11)	12.63 (0.12)	18.15 (0.18)	17.76 (0.28)	16.36 (0.09)
MnO										
Na_2O	0.05 (0.02)	0.09 (0.02)	0.05 (0.01)	0.08 (0.02)	0.08 (0.02)	0.08 (0.02)	2.07 (0.04)	0.03 (0.02)	0.03 (0.02)	0.04 (0.01)
K_2O										
P_2O_5										
S (ppm)	3801 (1346)	2003 (238)	894 (92)	7037 (983)	4944 (1143)	4734 (1390)	2113 (225)	4409 (208)	8793 (837)	4201 (408)
Total	99.80	98.03	98.08	100.62	100.19	99.78	97.48	98.89	100.11	98.92
Fe	64.73 (0.56)	0.07 (0.02)	0.05 (0.03)	63.12 (0.53)	64.54 (0.55)	64.63 (0.28)	62.29 (0.28)	62.68 (0.37)	62.91 (0.19)	64.71 (0.68)
Ni	0.03 (0.02)	0.08 (0.04)	70.19 (0.64)	0.06 (0.02)	0.06 (0.02)	0.04 (0.01)	0.36 (0.02)	0.03 (0.02)	0.03 (0.02)	0.06 (0.03)
Cu	0.08 (0.02)	74.04 (0.39)	0.05 (0.02)	0.10 (0.02)	0.11 (0.04)	0.11 (0.03)	0.30 (0.02)	0.14 (0.03)	0.11 (0.03)	0.16 (0.03)
S	34.17 (0.57)	21.94 (0.14)	27.53 (0.54)	35.57 (0.55)	34.39 (0.58)	33.77 (0.78)	35.33 (0.21)	36.09 (0.20)	36.02 (0.16)	33.28 (0.48)
O	1.87 (0.46)	n.d.	n.d.	0.68 (0.22)	1.45 (0.27)	2.05 (0.76)	0.56 (0.17)	0.25 (0.09)	n.d.	1.24 (0.17)
Total	100.88	96.13	97.82	99.54	100.55	100.60	98.84	99.19	99.06	99.45
S (calc.)[a]	4609 (1259)	1866 (510)	2334 (638)	7601 (2076)	5431 (1484)	5225 (1427)	2117 (578)	4355 (1190)	6291 (1719)	3112 (850)
S (calc.)[b]	4646 (1242)	2389 (639)	2298 (614)	7574 (2024)	5442 (1455)	5264 (1407)	2180 (583)	4372 (1169)	6308 (1686)	3154 (843)

(continued on next page)

701

Sample	C143	B291	B292	B293	0735	753	1605	1606	1607
SiO_2	42.84 (0.25)	47.88 (0.35)	45.08 (0.20)	47.76 (0.25)	45.77 (0.83)	51.94 (1.77)	40.74 (0.15)	42.75 (0.31)	34.36 (0.48)
TiO_2	0.02 (0.01)	0.02 (0.01)	0.01 (0.01)	0.03 (0.01)	0.02 (0.01)	0.21 (0.02)			
Al_2O_3	9.08 (0.13)	10.08 (0.06)	9.95 (0.06)	10.83 (0.12)	3.63 (0.07)	4.11 (0.53)	14.30 (0.06)	15.05 (0.14)	11.71 (0.16)
FeO	11.31 (0.26)	0.90 (0.04)	6.51 (0.08)	0.89 (0.02)	24.16 (0.89)	7.70 (1.64)	13.51 (0.17)	8.12 (0.1)	20.37 (0.75)
MgO	19.39 (0.30)	20.62 (0.11)	19.34 (0.21)	20.39 (0.2)	9.90 (0.16)	32.21 (2.34)	14.66 (0.06)	15.78 (.16)	15.38 (0.13)
CaO	15.93 (0.25)	18.25 (0.12)	17.17 (0.17)	18.20 (0.18)	10.28 (0.33)	1.29 (0.52)	14.95 (0.11)	16.12 (0.15)	14.21 (0.18)
MnO									
Na_2O	0.03 (0.02)	0.08 (0.01)	0.07 (0.01)	0.07 (0.01)	1.26 (0.04)	0.05 (0.03)	0.12 (0.01)	0.11 (0.01)	0.13 (0.01)
K_2O									
P_2O_5									
S (ppm)	2761 (165)	1380 (61)	694 (53)	969 (44)	4557 (947)	514 (73)	1455 (138)	1264 (123)	3568 (533)
Total	98.89	97.98	98.21	98.27	95.48	97.57	98.42	98.05	96.51
Fe	64.84 (0.84)	6.12 (0.16)	3.59 (0.43)	4.71 (0.20)	63.12 (0.52)	63.79 (0.75)	27.23 (3.12)	26.36 (1.92)	39.56 (2.58)
Ni	0.03 (0.02)	63.66 (0.59)	0.01 (0.02)	28.69 (8.95)	0.04 (0.02)	0.29 (0.03)	20.51 (2.84)	23.53 (2.22)	16.65 (2.86)
Cu	0.19 (0.02)	0.09 (0.02)	74.28 (3.35)	40.02 (9.57)	0.62 (0.04)	0.44 (0.04)	24.58 (4.75)	22.11 (3.57)	15.05 (1.24)
S	32.77 (1.23)	28.64 (0.25)	20.92 (2.58)	24.79 (0.82)	33.94 (0.49)	32.65 (0.59)	27.95 (1.09)	28.78 (0.68)	26.72 (1.48)
O	1.74 (1.07)	n.d.	n.d.	n.d.	2.12 (0.23)	2.46 (0.32)	1.04 (0.59)	0.63 (0.09)	3.40 (1.27)
Total	99.57	98.50	98.80	98.22	99.84	99.63	101.33	101.42	101.46
S (calc.)[a]	3085 (843)	1865 (510)	284 (78)	1441 (394)	6503 (1777)	418 (114)	1510 (413)	1379 (377)	2728 (745)
S (calc.)[b]	3141 (840)	1850 (495)	360 (96)	1624 (434)	6964 (1862)	470 (126)	1574 (421)	1417 (379)	2769 (740)

[a] Predicted concentration of sulfur in silicate melt using the ΔG^o of O'Neill and Mavrogenes (2002) assuming ideality in the sulfide solution.
[b] Predicted concentration of sulfur in silicate melt using the ΔG^o of O'Neill and Mavrogenes (2002) assuming non-ideality in the sulfide solution.
n.d. = none determined.

Table 3. Results of linear least-squares regression of experimentally determined sulfur solubilities in silicate melts

	Ideal (ΔG^o This Study)		Ideal (ΔG^o O+M 2002)		Non-ideal (ΔG^o O+M 2002)	
	Coefficient	Std. Error	Coefficient	Std. Error	Coefficient	Std. Error
A	-14683	(452)	-	-	-	-
B'	8.03	(0.25)	9.087	(0.25)	9.352	(0.25)
C	-265.80	(24.07)	-269.40	(24.17)	-264.85	(23.68)
A_{Si}	-	-	-27561	(500)	-27996	(500)
A_{Ti}	16430	(1465)	-11220	(1424)	-10715	(1398)
A_{Al}	9295	(811)	-18450	(794)	-19000	(788)
A_{Mg}	13767	(515)	-13970	(627)	-14512	(627)
A_{Ca}	19893	(737)	-7831	(856)	-8832	(871)
A_{Fe}	-7080	(2082)	-34274	(2376)	-34895	(2330)
A_{Na}	14197	(1441)	-13247	(1414)	-13713	(1388)
A_{K}	-	-	-29015	(2962)	-28584	(2900)
A_{H}	10189	(560)	-17495	(561)	-17766	(553)
$A_{Si\text{-}Fe}$	117827	(5474)	116568	(6066)	117816	(5943)
E	-	-	-	-	546	(129)

Table 4. Silicate melt compositions use for modeling of SCSS in Figures 2, 3 and 4.

	N-MORB[a]	Martian Basalt[b]	Andesite[c]	Komatiite[d]
SiO_2	50.42	45.50	56.52	46.80
TiO_2	1.53	0.60	1.08	0.26
Al_2O_3	15.13	6.70	17.54	4.50
FeO	9.81	17.90	7.65	11.00
MgO	7.76	14.30	4.06	29.60
CaO	11.35	9.30	7.40	5.21
Na_2O	2.83	0.70	3.94	0.28
K_2O	0.14	0.05	1.31	0.14

[a] Average N-MORB (Gale et al., 2013)
[b] Basaltic shergottite Dhofar019 (Bridges and Warren, 2006)
[c] Average andesite (Wilkinson, 1986)
[d] Barberton komatiite B95-18 (Parman et al., 2003)

702

This is a preprint, the final version is subject to change, of the American Mineralogist (MSA)
Cite as Authors (Year) Title. American Mineralogist, in press.
(DOI will not work until issue is live.) DOI: http://dx.doi.org/10.2138/am-2017-5800CCBY

Figure 1

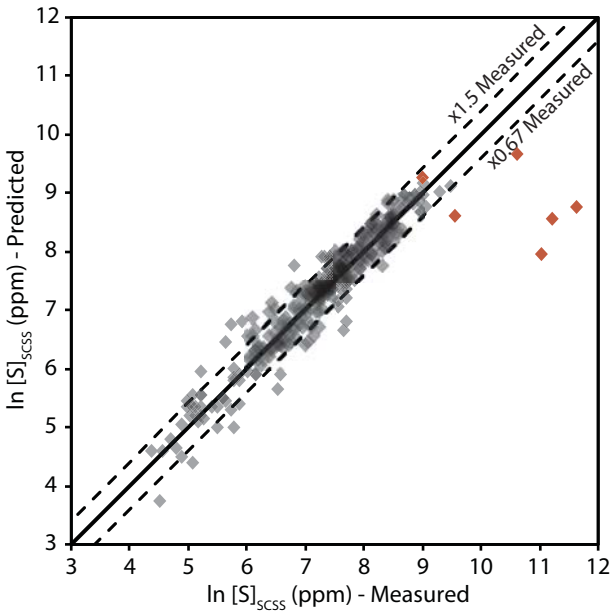

This is a preprint, the final version is subject to change, of the American Mineralogist (MSA)
Cite as Authors (Year) Title. American Mineralogist, in press.
(DOI will not work until issue is live.) DOI: http://dx.doi.org/10.2138/am-2017-5800CCBY

Figure 2

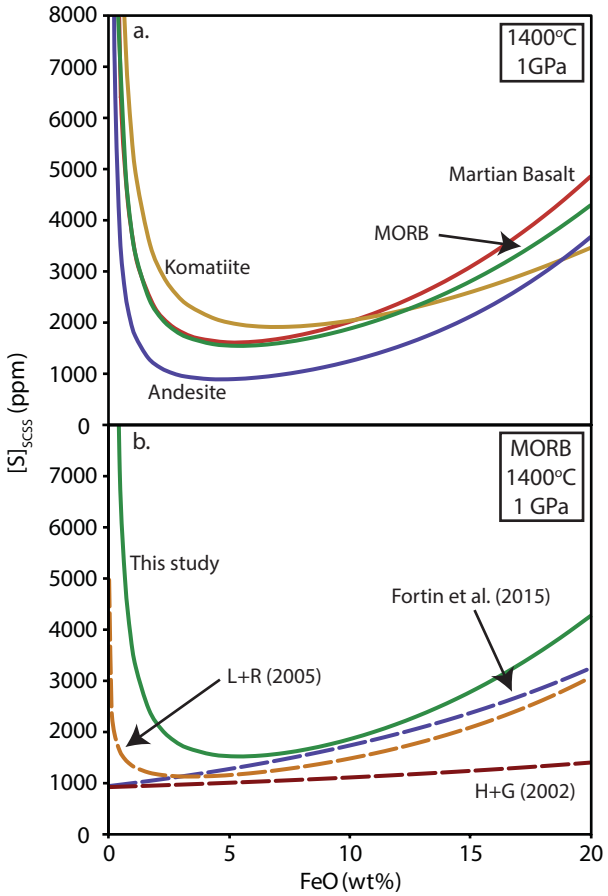

This is a preprint, the final version is subject to change, of the American Mineralogist (MSA)
Cite as Authors (Year) Title. American Mineralogist, in press.
(DOI will not work until issue is live.) DOI: http://dx.doi.org/10.2138/am-2017-5800CCBY

Figure 3

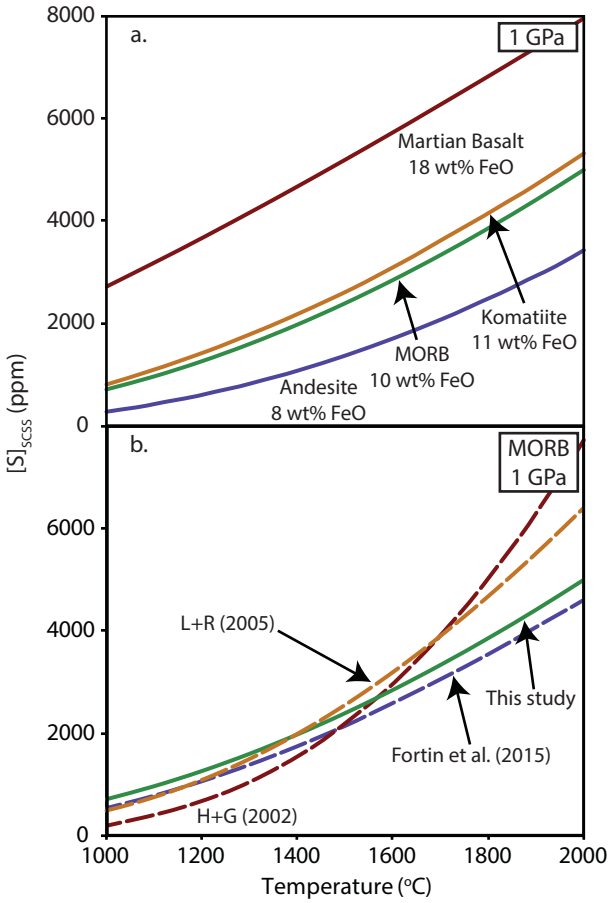

This is a preprint, the final version is subject to change, of the American Mineralogist (MSA)
Cite as Authors (Year) Title. American Mineralogist, in press.
(DOI will not work until issue is live.) DOI: http://dx.doi.org/10.2138/am-2017-5800CCBY

Figure 4

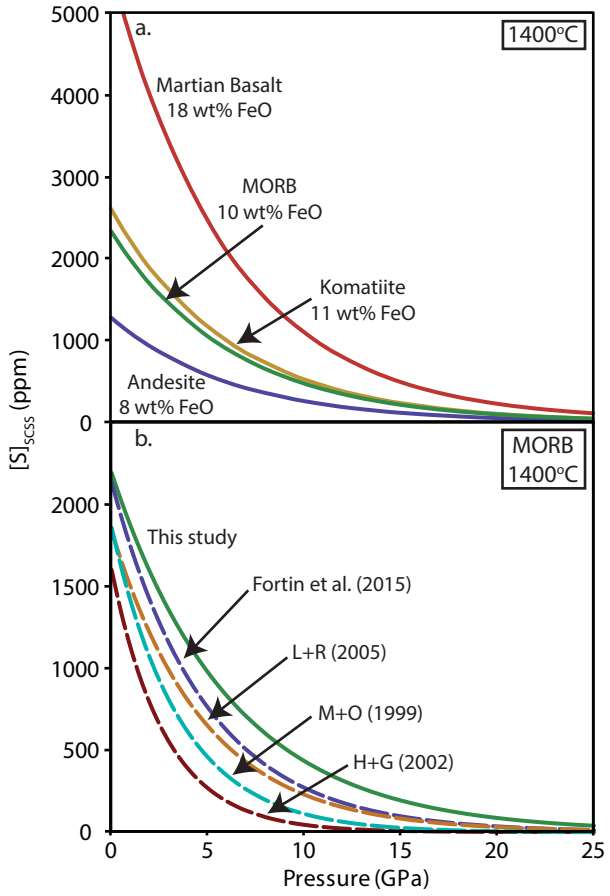

This is a preprint, the final version is subject to change, of the American Mineralogist (MSA)
Cite as Authors (Year) Title. American Mineralogist, in press.
(DOI will not work until issue is live.) DOI: http://dx.doi.org/10.2138/am-2017-5800CCBY

Figure 5

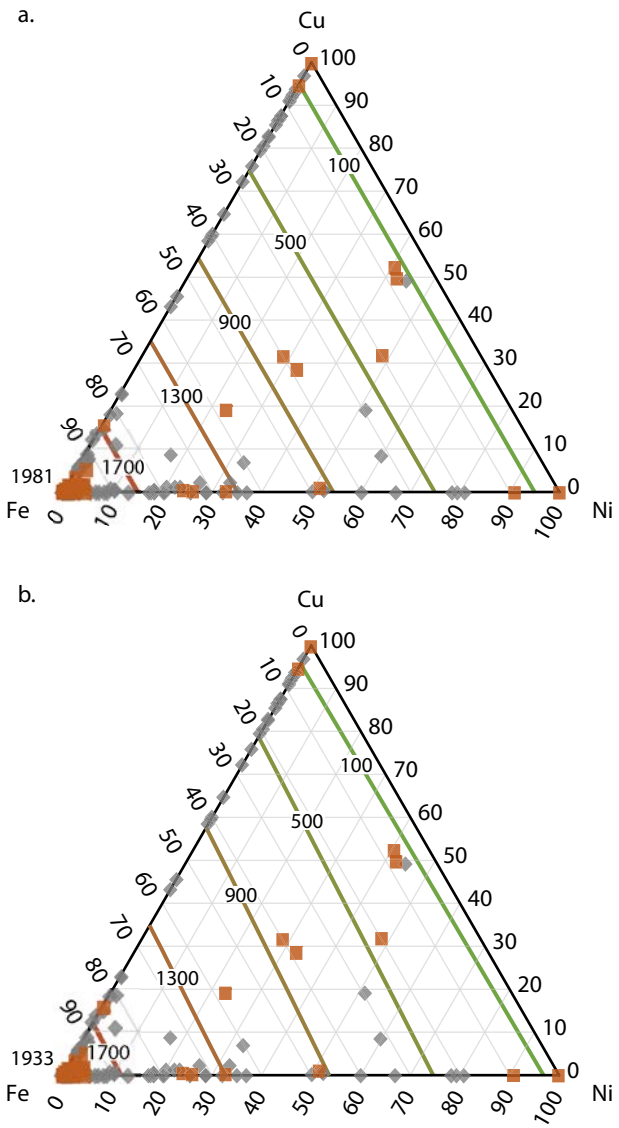

This is a preprint, the final version is subject to change, of the American Mineralogist (MSA)
Cite as Authors (Year) Title. American Mineralogist, in press.
(DOI will not work until issue is live.) DOI: http://dx.doi.org/10.2138/am-2017-5800CCBY

Figure 6